www.ietdl.org

Published in IET Electric Power Applications
Received on 29th March 2014
Revised on 9th July 2014
Accepted on 18th July 2014
doi: 10.1049/iet-epa.2014.0115

ISSN 1751-8660

Adaptive sliding mode technique-based electromagnetic suspension system with linear switched reluctance actuator

Jiongkang Lin[1], Ka Wai Eric Cheng[1], Zhu Zhang[2], Norbert C. Cheung[1], Xiangdang Xue[1]

[1]*Department of Electrical Engineering, Hong Kong Polytechnic University, Hung Hom, Kowloon, Hong Kong*
[2]*School of Information and Electrical Engineering, Hunan University of Science and Technology, China*
E-mail: eeecheng@polyu.edu.hk

Abstract: Linear switched reluctance actuator (LSRA) is of great potential using in kind of high-force linear applications such as automotive suspension system. In this study, an electrical controlled active suspension system is built. Bi-directional power amplifier is used to supply power to and absorb generated energy from linear actuator based on the movement requirement. The linear motions are accomplished by retracting and extending the LSRA. With regard to the established electromagnetic suspension system, a real-time control algorithm is developed. Sliding model technique with adaptive mechanism is studied to compensate the system non-linearities and external road profile. Experiments are conducted at the laboratory to present the high performance of proposed active suspension system.

1 Introduction

Since the first installation of electro-hydraulic actuators to Lotus race car recorded in 1980s, active suspension system has increasingly attracted more interest. The superior performance of active suspension system is the main attractive attribute, including short response time and flexible control method [1–5]. Nowadays, hydraulic active suspension system is the mainstream of commercial applications. The remarked active body control system can adjust the body movement of the vehicle and achieve self-levelling with regard to various driving situations by applying hydraulic servomechanism. However, the hydraulic servomechanism is an expensive and complicated mechanical system with slow response time and high energy consumption. The development of active suspension system is to pursue improved performance and fast response time, while the mechanical structure and cost can be reduced relevantly [4, 6].

Developing reliable and feasible electromagnetic active suspension systems has been one of the research focuses of automotive industry. Electromagnetic system is more reliable and has the potential to replace the electro-hydraulic system. The mechanical structure of electromagnetic system is significantly simplified by replacing the hydraulic valves with electrical actuators [7–10]. Furthermore, it is benefited by the distinct properties of electrical actuators including extremely fast response and high energy efficiency [11–13]. Among the developed linear electrical actuators, linear permanent magnet synchronous motor (LPMSM) is of the highest performance [14]. Up to now, LPMSMs provide highest force density and lowest force per watt of losses because of the existence of high performance permanent magnet material, such as NdFeB magnet. However, the NdFeB magnet is expensive that leads the actuator's initial cost relatively high. Moreover, demagnetisation is a main drawback of NdFeB magnet when the ambient temperature is around 150°C or above. The suspension system is usually working under such tough environment. Hence, the environmental temperature to the suspension is a factor that affects the performance of the LPMSM. Comparing with the LPMSM, there is no permanent magnet in the linear switched reluctance actuator (LSRA) that makes the LSRA be a suitable candidate for harsh operating environment. Besides, LSRA has the advantage of simple structure, robust, low cost and maintenance free [14–19].

An electromagnetic active suspension system with LSRA is presented in this research. The proposed active suspension module can be divided into two parts: mechanical part that is composed of the LSRA and coil spring in parallel to sustain the car body and suppress the vertical vibration; electrical part supplies power to the linear actuator in a specific sequence that generates the required force and achieve desired performance, including a bi-directional power amplifier, a set of batteries and capacitor bank and real-time controller.

The most remarkable advantage of active suspension system is the establishment of active actuator to provide external force and eliminate trade-off between handling safety and driving comfort. Therefore, the performance of active suspension system is determined by the control methods and their implementation. Although the structure of electromagnetic system has been significantly simplified with regard to other types of active suspension system, the electrical–mechanical system is an instinctively complicated system with non-linearities [20]. Thus, non-linear control

methods and intelligent control methods are suitable for the sophisticated active suspension system. Non-linear control methods including sliding mode control and adaptive control have been investigated for decades to deal with non-linear time-varying system [21–24]. Sliding mode control is widely used to deal with non-linearities of suspension system [20, 25–29]. The sliding mode controller is used to generate the required active force and stable the car body regardless of road vibration. In [27], an adaptation scheme is designed to regulate the proportional-integral-derivative (PID) gains of the controller for the purpose of accommodating actuator faults. A non-linear quarter-car model is proposed in [20] with the consideration of non-linear spring characteristics. The function approximation technique is used to estimate the unknown system parameters and uncertainties. Besides, fuzzy logic is used to present the system model and improve the system stability. Takagi–Sugeno fuzzy rule is employed to establish the non-linear system model via the sector non-linearity approach in [2]. An adaptive sliding mode scheme is proposed to reach the specified sliding surface satisfied with the asymptotical stability. The global stability of controlled system can be improved through an enhanced adaptive self-organising fuzzy sliding mode controller [30] for active suspension system. By using a sliding surface and its derivative as the inputs of the fuzzy logic controller, the improved stability of the proposed method is proven via the Lyapunov stability theorem.

In this research, an adaptive sliding mode control for non-linear quarter-car suspension system is proposed. Based on the previous developed [9] LSRA, the related power amplifier is fabricated to achieve direct drive of LSRA. The system dynamic model is derived with the consideration of non-linear spring property. Sliding mode technique is applied to deal with the system non-linearities for its simplicity and robust. In practical system, the system parameters and load of the suspension are unknown. An adaptive mechanism is added to estimate the upper bound of the system perturbation. Stability of the controlled system can be guaranteed without any knowledge of the suspension system.

In this paper, detailed design of a quarter-car active suspension system with LSRA is described at the beginning. The models of the electromagnetic suspension system and the LSRA are obtained for the purpose of control. An adaptive sliding mode control method is developed to deal with the external road disturbance and parameters variation. The stability and robustness of the proposed control method are analysed. The performance of the prototype is verified at the laboratory platform to illustrate the effectiveness of the proposed control method.

2 Design of the quarter-car active suspension system

2.1 Power amplifier

An overview of the quarter-car active suspension system is figured out in Fig. 1. The power of the whole module is derived from the battery or DC link. The voltage of DC link is selected as 48 V to meet the existed battery configuration in most vehicles. The phase shift converter is used to boost low battery voltage of 48 V to high switched reluctance actuator input voltage at 150 V. The power amplifier module is used to monitor and operate the active suspension system. Bi-directional topology provides two modes of power flow: normal mode that injects the energy into the actuator and drive the system; regenerating mode that extracts energy to the capacitor bank and save energy consumption. The capacitor bank is used to store the recursive energy and provide extra power for instantaneous high force. LSRA is employed to generate active force and implement linear motion. The electric signals and position signals are sensed and filtered by the sensing circuit, and then fed back to the real-time controller. The real-time controller monitors the active suspension system and suppresses the system oscillation by regulating the LSRA.

2.2 Linear switched reluctance actuator (LSRA)

LSRA is well known for its simple structure, robustness, low cost and free of maintenance. The structure of the proposed LSRA is outlined in Fig. 2. Fig. 2*a* shows that the proposed LSRA is composed of four parallel double-sided modules with shared shaft in a compact arrangement. The lateral forces of the LSRA modules are balanced through the symmetric configuration. High thrust is generated by four modules in parallel. The detailed structure of LSRA modules is depicted in Fig. 2*b*. The double-sided LSRA module is composed of eight pairs of stator poles and eight translator poles. The selection of four-phase topology aims to reduce force ripple. There is no permanent magnet, excitation windings and back iron installed in the translator. Thus the weight of the translator that is a part of the system load can be reduced to enhance the capability of the active suspension system.

The design of LSRA is preceded through magnetic circuit analysis and finite element analysis (FEA) with the consideration of physical requirements and constraints. The stroke is the maximum safe travel distance between the sprung mass and unsprung mass. In order to absorb the road irregularities and ensure the function and safety of the

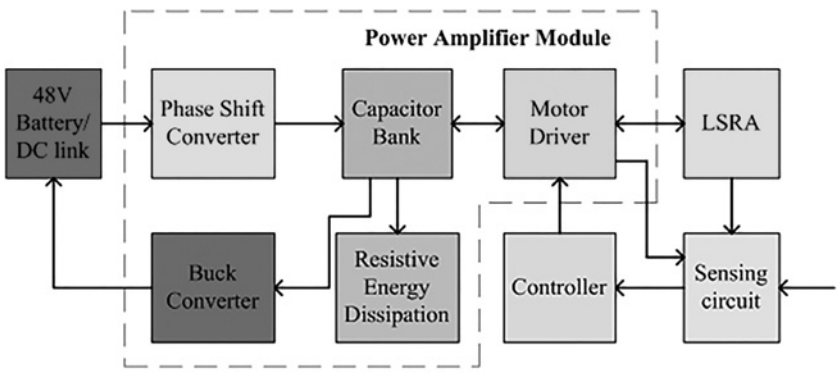

Fig. 1 *Diagram of the quarter-car active suspension system*

Table 1 Specification per LSRA module

Quantity	Value	Quantity	Value
number of modules	4	number of phases	4
number of stator pole pairs per module	8	number of translator poles	8
stator pole pitch	36 mm	translator pole pitch	48 mm
stator pole width	13 mm	translator pole width	17 mm
stator pole height	49 mm	stator yoke thickness	13 mm
stack length	43 mm	stroke	96 mm (±48 mm)
nominal voltage	150–200 V	nominal current	10 A
peak power	4800 W		
nominal force	125 N	peak force	500 N

active suspension system, the stroke value is selected as 96 mm (upward/downward 48 mm).

The demand active force generated by the LSRA mainly depends on the sprung mass, road profiles and required performance. Higher force provides more comfort and safety in which requires larger volume. Compromise between the volume and output active force is considered. According to ISO2631 about human reaction to vibration magnitudes, the peak force is decided as 2000 N per system and 500 N per module, and the continuous force is 500 N per system and 125 N per module.

The volume constraint is decided by the vehicle grade and existing available room space. Through extensive investigation of medium-volume vehicle and related suspensions, the volume of the proposed LSRA is constrained as 300 mm × 300 mm × 600 mm.

On a basis of the predefined output force and maximum volume, the parameters of linear actuator are calculated by magnetic circuit analysis and optimised by FEA. The optimisation procedure is conducted in [31]. The optimised parameters of LSRA module is specified in Table 1 [3].

2.3 Test rig

The prototype of the test rig has been fabricated and assembled for examining the performance of the active

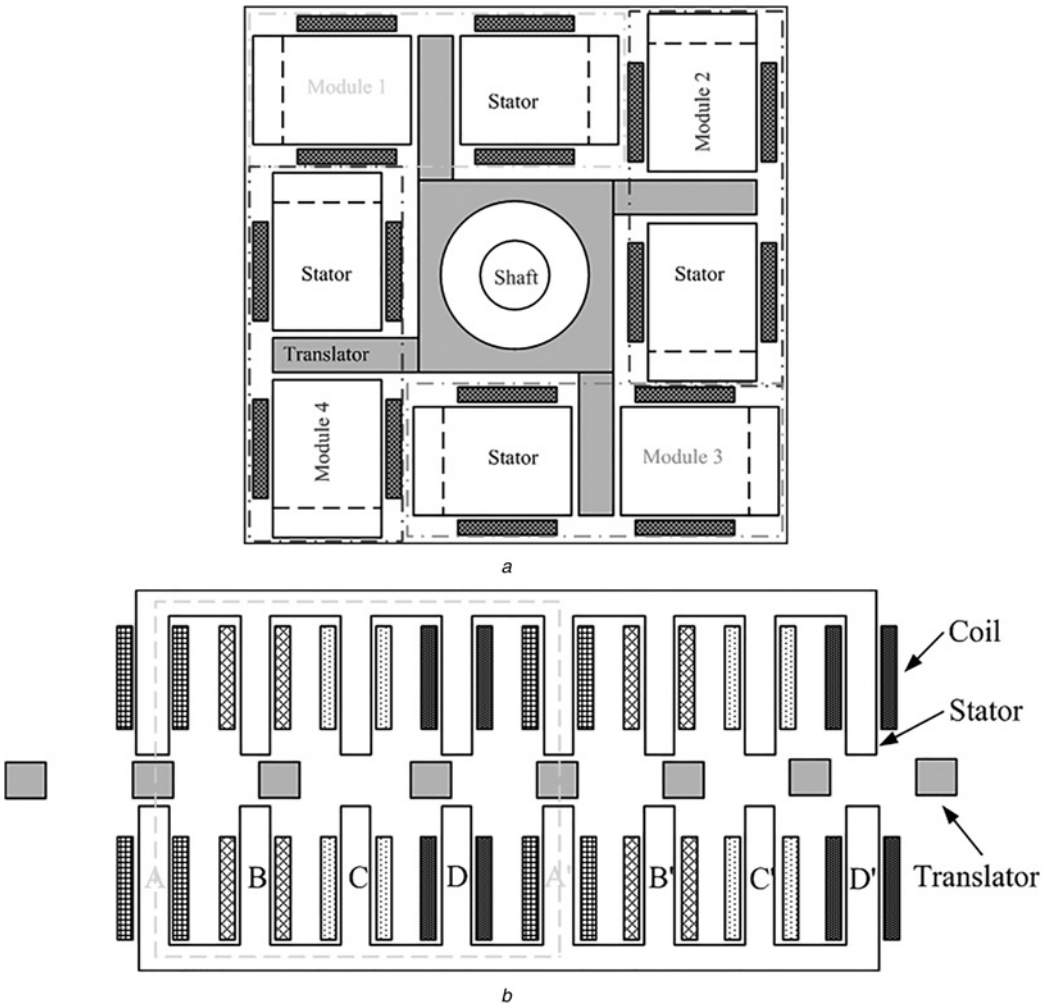

Fig. 2 *Structure of the LSRA*

a Transverse structure (four modules in parallel)
b Longitudinal structure (double-sided four-phase module)

doi: 10.1049/iet-epa.2014.0115

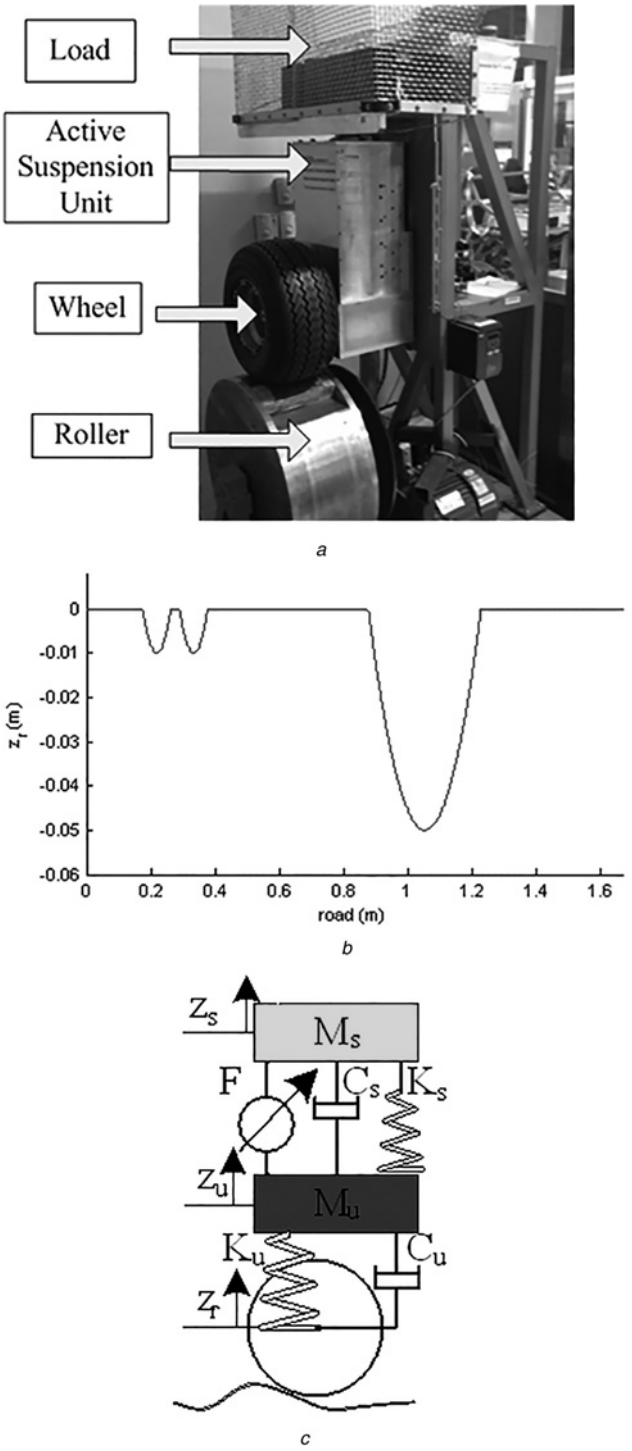

Fig. 3 *Quarter-car active suspension system*

a Test rig
b Road profile
c Model

suspension system and related control algorithms. Fig. 3*a* shows the test rig equipped with active suspension module. The rolling drum is driven by induction motor that is behind the rolling drum and unseen in the photo. Once the drum rolls, the tyre runs on the surface of the drum to simulate longitudinal movement of the vehicle. Uneven road surface induces vibration and oscillation to both the sprung mass subsystem and unsprung mass subsystem of the quarter-car system. Then the active suspension system is activated to generate force to suppress these movements and keep the sprung mass subsystem stable. The road profile is a periodically surface with three isolated bumps, which is described in Fig. 3*b*.

3 System model

3.1 Non-linear quarter-car model

The model of the proposed quarter-car active suspension system is illustrated in Fig. 3*c*. The car body is represented by sprung mass M_s that is sustained by passive components of equivalent damper C_s and non-linear spring K_s and active component of LSRA. The unsprung mass M_u is the assembly of chassis and wheel. The whole system is supported by the wheel that can be expressed as a linear spring K_u in parallel with a damper C_u. The active force F of LSRA is used to absorb the vibration of sprung mass part regardless of road irregularities. The output force of LSRA is constrained by the mechanical bearing and electromagnetic field, that is, $F \in \left[-F_{\max} \quad F_{\max} \right]$ and $F_{\max} > 0$ is the maximum output force. The road profile is represented as z_r which is injected to the wheel and cause the oscillation of unsprung masses z_u and then sprung mass z_s with regard to the undeformed positions.

The spring coefficient K_s is a combination of linear stiffness K_{1s} and non-linear stiffness K_{2s}. Thus, the system dynamic can be modelled as following (see (1))

$$\begin{cases} M_s\ddot{z}_s = -K_{1s}(z_s - z_u) - K_{2s}(z_s - z_u)^3 - C_s(\dot{z}_s - \dot{z}_u) + F - M_s g \\ M_u\ddot{z}_u = K_{1s}(z_s - z_u) + K_{2s}(z_s - z_u)^3 + C_s(\dot{z}_s - \dot{z}_u) - K_u(z_u - z_r) - C_u(\dot{z}_u - \dot{z}_r) - F - M_u g \end{cases} \tag{1}$$

where g is the gravity constant. The reference positions of sprung and unsprung masses are calculated at the static condition: $z_{u0} = -((M_s + M_u)/K_u)g$ and $z_{s0} = z_{u0} + z_0$ with $K_{1s}z_0 + K_{2s}z_0^3 + M_s g = 0$. The initial positions z_{s0} and z_{u0} are highly parameter-dependant and can be measured by the position sensors in practical system. Define the state variables as $x_1 = z_s - z_{s0}$, $x_2 = \dot{z}_s$, $x_3 = z_u - z_{u0}$ and $x_4 = \dot{z}_u$, the system dynamic of (1) can be rewritten as (see equation (2) on the bottom of the next page).

In contrast to the constant unsprung mass M_u, the vehicle load is consistent during individual testing, and it varies from time to time that is constrained by the maximum load. Suppose the nominal sprung mass is M_{s0}, the time-varying sprung mass is $M_s = M_{s0} + \Delta M_s$ with load variation ΔM_s. Besides, the precise values of system parameters are not constant during operating and vary with load variations and system non-linearities. Similar to sprung mass, the nominal values of spring stiffness and damper are K_{1s0}, K_{2s0} and C_{s0}, and the actual values are $K_{1s} = K_{1s0} + \Delta K_{1s}$, $K_{2s} = K_{2s0} + \Delta K_{2s}$ and $C_s = C_{s0} + \Delta C_s$, respectively.

At the laboratory test platform, only the sprung mass position $x_1 = z_s - z_{s0}$ is measured, and its derivative $x_2 = \dot{z}_s$ can be obtained through a non-linear tracking-differentiator. Suppose $z = x_1$, the system dynamic for control purpose is simplified as

$$\ddot{z} = f(x, t) + b(t)F \tag{3}$$

where $x = \begin{bmatrix} x_1 & x_2 & x_3 & x_4 \end{bmatrix}^{\mathrm{T}}$ is the state vector, $b(t) = 1/(M_s(t))$ and

$$f(x, t) = \frac{1}{M_s(t)}\left[-K_{1s}(t)(x_1 - x_3) - K_{2s}(t)(x_1 - x_3)^3 - C_s(t)(x_2 - x_4)\right]$$

3.2 LSRA model

The dynamic model of LSRA based on voltage balancing principle is represented as

$$\frac{\mathrm{d}i_j}{\mathrm{d}t} = -\frac{R_s}{L_j}i_j - \frac{v}{L_j}\frac{\mathrm{d}L_j}{\mathrm{d}s}i_j + \frac{1}{L_j}u_j, j = a, b, c, d \quad (4)$$

where u_j and i_j is phase voltage and phase current, R_s and L_j is related resistance and inductance, $\lambda_j = L_j i_j$ is phase flux linkage, respectively. s is translator displacement while $v = \dot{s}$ is its velocity. It needed to point out that the LSRA is a highly non-linear actuator, the phase inductance is a function of position and phase current with the form of $L_j(s, i_j)$.

The actuator force dynamic F_a is expressed as a function of the phase currents and corresponding inductance profiles

$$F_a = \sum_j \frac{1}{2}\left(\frac{\mathrm{d}L_j}{\mathrm{d}s}\right)i_j^2, j = a, b, c, d \quad (5)$$

The dynamic characteristics of the proposed LSRA are depicted in Fig. 4. It can be observed that the dynamics are highly non-linear and varied with translator position and phase currents. The mechanical period is 48 mm that is half of the suspension stroke. When the current is constant, the inductance and flux profiles have their maximum values at the point of 24 mm that is the central point of the period while the output force is zero. The LSRA generates positive force in the first half [0 mm, 24 mm] when the inductance has positive derivative and reaches its maximum value at 24 mm; during the second half [24 mm, 48 mm] the inductance decreases from its maximum point to minimum point and the LSRA generates negative force.

4 Adaptive sliding mode control and its analysis

An adaptive sliding mode control algorithm is developed here to suppress the oscillation of sprung mass. The closed-loop stability and robustness of the proposed method is analysed thereafter.

4.1 Control method

Define the dynamic of the closed-loop quarter-car active suspension system as

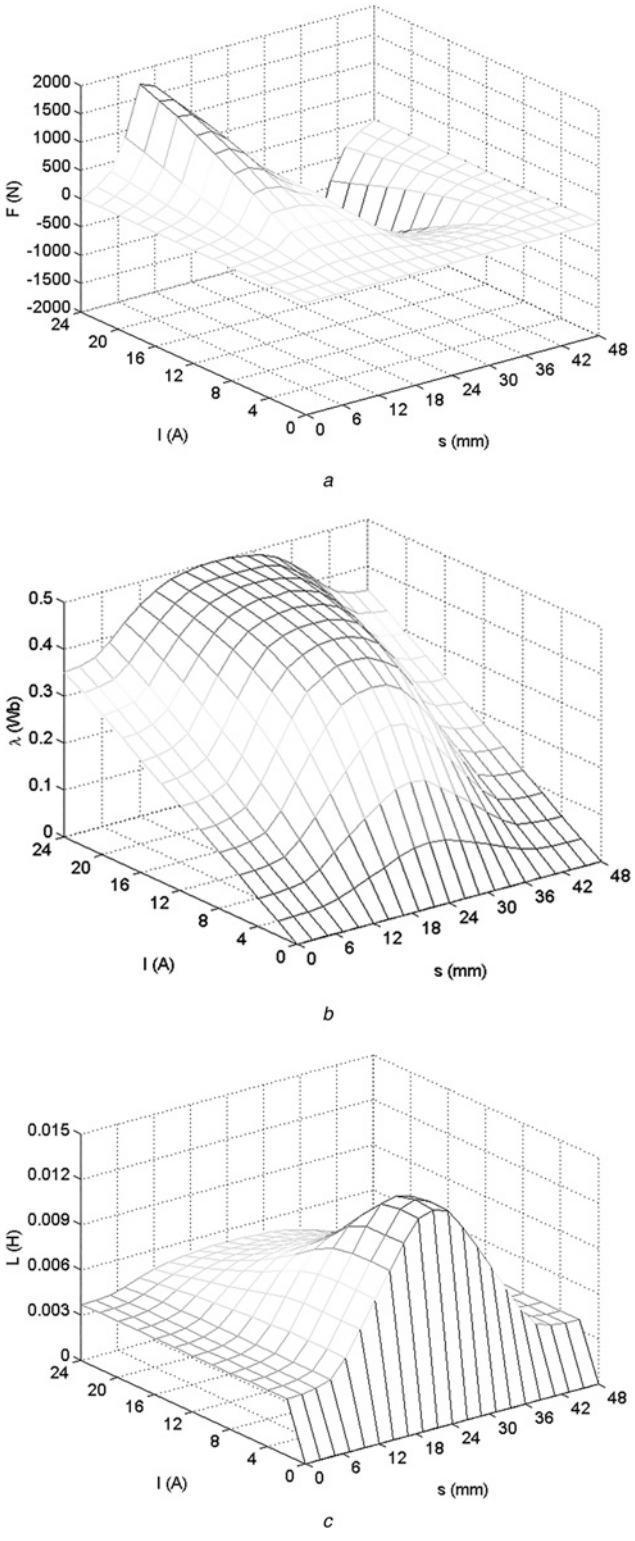

Fig. 4 *Characteristic of LSRA module*

a Force characteristics
b Flux characteristics
c Inductance profile

$$\begin{cases} \dot{x}_1 = x_2 \\ \dot{x}_2 = \dfrac{1}{M_s}\left[-K_{1s}(x_1 - x_3) - K_{2s}(x_1 - x_3)^3 - C_s(x_2 - x_4)\right] + \dfrac{F}{M_s} \\ \dot{x}_3 = x_4 \\ \dot{x}_4 = \dfrac{1}{M_u}\left[K_{1s}(x_1 - x_3) + K_{2s}(x_1 - x_3)^3 + C_s(x_2 - x_4) - K_u(x_3 - z_r) - C_u(x_4 - \dot{z}_u)\right] - \dfrac{F}{M_u} \end{cases} \quad (2)$$

doi: 10.1049/iet-epa.2014.0115

$$\sigma = \dot{z} + pz \tag{6}$$

where $p > 0$ is the slope of the sliding surface. To suppress the sprung mass vibration $z = 0$, the sliding mode is needed to converge to zero. The derivative of sliding surface is

$$\dot{\sigma} = \ddot{z} + p\dot{z} \tag{7}$$

Substituting (3) into (7), the sliding mode dynamic can be expressed as

$$\begin{aligned}\dot{\sigma} &= f(x, t) + b(t)F + p\dot{z} \\ &= p\dot{z} + b_0F + \big(f(x, t) + \big(b(t) - b_0\big)F\big) \\ &= p\dot{z} + b_0F + d\end{aligned} \tag{8}$$

where $d = f(x, t) + (b(t) - b_0)F$ is the generic disturbance of the controlled system.

The force F of linear sliding mode control contains two parts: nominal force F_0 and discontinuous force F_d. The form of the control law is

$$\begin{cases} F = F_0 + F_d \\ F_0 = -\dfrac{1}{b_0}p\dot{z} \\ F_d = -\gamma_1\sigma - \gamma_2\text{sign}(\sigma) \end{cases} \tag{9}$$

where γ_1 and γ_2 are positive gains. Generally speaking, larger control gains have greater potential of stabilising system. However, too large gains can cause system chattering. In conjunction with the estimate of d, the system error can be reduced significantly and thus the control gains can be selected relatively small. Furthermore, only the bound of disturbance is involved in the control output can enhance the system robustness. Suppose the upper bound of system disturbance using function approximation technique is

$$\zeta = \alpha^{\mathrm{T}}\rho \tag{10}$$

where $\rho = \begin{bmatrix} |z| & |\sigma| \end{bmatrix}^{\mathrm{T}}$, $\alpha = \begin{bmatrix} \alpha_1 & \alpha_2 \end{bmatrix}^{\mathrm{T}}$ with $\alpha_1, \alpha_2 > 0$.

The adaptive control law is

$$F = -\frac{1}{b_0}p\dot{z} - \gamma_1\sigma - M_{s\max}\hat{\alpha}^{\mathrm{T}}\rho\text{sign}\big(\sigma\hat{\alpha}^{\mathrm{T}}\rho\big) \tag{11}$$

where $\hat{\alpha} = \begin{bmatrix} \hat{\alpha}_1 & \hat{\alpha}_2 \end{bmatrix}^{\mathrm{T}}$ is the estimate of α. The update law of $\hat{\alpha}$ is

$$\dot{\hat{\alpha}} = Q^{-1}|\sigma|\rho \tag{12}$$

where Q is a symmetric positive definite matrix.

4.2 Stability

To prove the closed-loop system stability and the asymptotic convergence of sliding surface, the Barbalat's Lemma [16] is employed. The Lyapunov function is defined as

$$V = \frac{1}{2}b_0\sigma^2 + \frac{1}{2}\tilde{\alpha}^{\mathrm{T}}Q\tilde{\alpha} \tag{13}$$

where $\tilde{\alpha} = \hat{\alpha} - \alpha$ is the estimate error of α. The time derivative of the Lyapunov function incorporating (8), (11) and (12) is

$$\begin{aligned}\dot{V} &= \sigma\dot{\sigma} + \tilde{\alpha}^{\mathrm{T}}Q\dot{\hat{\alpha}} \\ &= \sigma\big(p\dot{z} + b_0F + d\big) + \tilde{\alpha}^{\mathrm{T}}QQ^{-1}|\sigma|\rho \\ &= \sigma\big(-b_0\gamma_1\sigma - b_0M_{s\max}\hat{\alpha}^{\mathrm{T}}\rho\text{sign}\big(\sigma\hat{\alpha}^{\mathrm{T}}\rho\big) + d\big) + \tilde{\alpha}^{\mathrm{T}}|\sigma|\rho \\ &= -b_0\gamma_1\sigma^2 + \sigma\big(-b_0M_{s\max}\hat{\alpha}^{\mathrm{T}}\rho\text{sign}\big(\sigma\hat{\alpha}^{\mathrm{T}}\rho\big) + d\big) + \tilde{\alpha}^{\mathrm{T}}|\sigma|\rho \\ &\le -b_0\gamma_1\sigma^2 - b_0M_{s\max}\sigma\hat{\alpha}^{T}\rho sign\big(\sigma\hat{\alpha}^{\mathrm{T}}\rho\big) + \sigma\alpha^{\mathrm{T}}\rho + \tilde{\alpha}^{\mathrm{T}}|\sigma|\rho \\ &= -b_0\gamma_1\sigma^2 - b_0M_{s\max}|\sigma|\hat{\alpha}^{\mathrm{T}}\rho + \sigma\alpha^{\mathrm{T}}\rho + \tilde{\alpha}^{\mathrm{T}}|\sigma|\rho \\ &\le -b_0\gamma_1\sigma^2\end{aligned} \tag{14}$$

With the control law of (14), the Lyapunov function (13) will converge to zero asymptotically. Thus, the sliding surface σ and the estimate error α will converge to zero in a finite time.

4.3 Robustness

To improve the robustness of the active suspension system, the force error is considered. The difference between the ideal force command and actual force output is because of the electro-mechanical output force non-linearity, time-delay of inner current tracking loop and system parameter mismatch.

In the above discussion, the controller desired force F equals the LSRA output force F_a. However, a force error exists in actual application. The actual output force is

$$bF_a = b_0F + b_0(F_a - F) + (b - b_0)F \tag{15}$$

where the left side is the actual force input of the active suspension system. The right side can be divided into three parts: (i) nominal output force of the controller; (ii) force error because of time-delay; and (iii) force error because of system parameters variation. The robustness of the system can be enhanced by covering the second and third terms.

The sliding surface dynamic (8) is rewritten as

$$\begin{aligned}\dot{\sigma} &= f(x, t) + b(t)F + p\dot{z} \\ &= p\dot{z} + b_0F + \big(f(x, t) + b_0(F_a - F) + \big(b(t) - b_0\big)F\big) \\ &= p\dot{z} + b_0F + d_a\end{aligned} \tag{16}$$

where $d_a = f(x, t) + b_0(F_a - F) + (b(t) - b_0)F$ is the generic disturbance of the controlled system.

Since the generic disturbance d_a is bounded in physical system, the system can be stabilised through the control law (11) and (12) in a finite time. In the other side, it can be observed that the last two terms of d_a are determined by the forces F, F_a and sprung mass M_s. Thus, parts of the bound d_a can be expressed by a function of M_{s0} and F, that is

$$\big|b_0(F_a - F) + \big(b(t) - b_0\big)F\big| \le \frac{\Delta_{\mathrm{F}}}{M_{s0}}F + \frac{\Delta_{M_s}}{M_{s0}}F \tag{17}$$

where Δ_{F} is the force error between the desired force and actual force that is related to the actuator drive dynamic; Δ_{M_s} is the variation of sprung mass. In this research, Δ_{M_s} is constrained as 0.2; Δ_{F}, a term determined by the inner current loop, is less than 0.2 by PI control. The global stability of (13) can be guaranteed by adding force

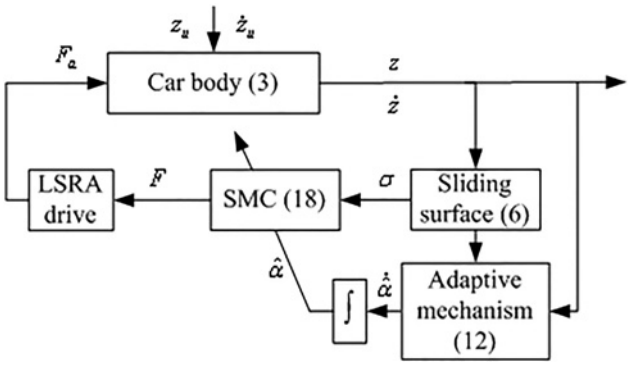

Fig. 5 *Control scheme of adaptive sliding mode control*

compensation part into (11) as follows

$$F = -\frac{1}{b_0}p\dot{z} - \gamma_1\sigma - \Delta\text{sign}(\sigma) - M_{s\max}\hat{\alpha}^{\mathrm{T}}\rho\text{sign}\left(\sigma\hat{\alpha}^{\mathrm{T}}\rho\right) \quad (18)$$

where $\Delta = (\Delta_{\mathrm{F}} + \Delta_{Ms})F_k$ and F_k is the previous output force.

The output force under adaptive sliding mode control (SMC) is expressed in (18). As we know, chattering problem is an issue considered in sliding mode control because of the introduction of signum function. One simple and effective method is the boundary layer solution [21], that is, replace the signum function with saturation function to avoid control discontinuities and switching action. An alternative method is super twisting SMC [24]. According to [29], the chattering problem can be reduced significantly through the second-order sliding mode control method.

The control scheme of adaptive sliding mode control is depicted in Fig. 5. The sliding surface determines the dynamic σ of the closed-loop quarter-car active suspension system by slope p. In conjunction with the system dynamic and sliding surface, the adaptive mechanism $\hat{\alpha}$ is obtained. Thus, the desired output force is generated by sliding mode technology. A direct drive LSRA is used to output actual force and stabilise the car body of active suspension system in regardless of system uncertainties and road variation.

5 LSRA drive

A typical LSRA drive is illustrated in Fig. 6. The desired output force F is used to generate the demand currents of LSRA in conjunct with inductance derivatives. The inner current loop traces the demand phase currents and then generates the required electromagnetic force F_a through PI control. The fine-tuned parameters of PI control gains can ensure the current fast tracking smoothly. The look-up table of inductance derivative against position and current is derived by FEA data and examined by experiment.

As discussed in Section 4.3, the faster current tracking is achieved the less Δ_{F} is obtained. The input error e_i can be obtained by $e_i = i^* - i$, the required terminal voltage is calculated as

$$u^* = k_p e_i + k_i \int e_i \mathrm{d}t \quad (19)$$

where k_p and k_i are the proportional and integral gain of inner current PI controller. A tuning rule denoted as approximate M-constrained integral gain optimisation (AMIGO) is developed to explore the simple relationship between process parameters and the control parameters through a large test batch of process [32]. By using AMIGO, the controller gains k_p and k_i can be evolved analytically to enhance the robustness of the PI controller. Here, the proportional gain is set to be $k_p = 200$, the integral gain can be calculated as $k_i = k_p \cdot T/T_s$, in which T is the sampling period of 20 kHz, T_s is the settling time and is set to be $T_s = 0.002$ s.

Table 2 Parameters of adaptive SMC controller

Symbol	Value	Symbol	Value
p	10	γ_1	5
Δ_{M_s}	0.2	Δ_{F}	0.1
Q	$\begin{bmatrix} 5 & 0 \\ 0 & 1 \end{bmatrix}$	$\hat{\alpha}(0)$	$\begin{pmatrix} 0 & 0 \end{pmatrix}$

6 Simulation and experimental results

In this section, the proposed adaptive sliding mode control method is examined in both simulation and experiment. First of all, the control gains are needed to be fixed. The dynamic slope is set to be $p = 10$ to achieve fast dynamic. The load variation is within 20 kg, thus $\Delta_{M_s} = 0.2$. Δ_{F} is mainly determined by the PI tracking performance of current loop. As per the PI control gains of inner loop listed in Section 5, the related Δ_{F} is less than 0.1, while the outer loop frequency is 4 kHz, that is, $\Delta_{\mathrm{F}} = 0.1$. The symmetric positive definite matrix Q determines the convergence velocity of $\hat{\alpha} \to \alpha$, and is set to be $Q = \begin{bmatrix} 5 & 0 \\ 0 & 1 \end{bmatrix}$ implies that the position signal converges faster than the speed signal. Without the loss of generality, initial value $\hat{\alpha}(0)$ is set to be $\begin{pmatrix} 0 & 0 \end{pmatrix}$. The control parameters are listed in Table 2.

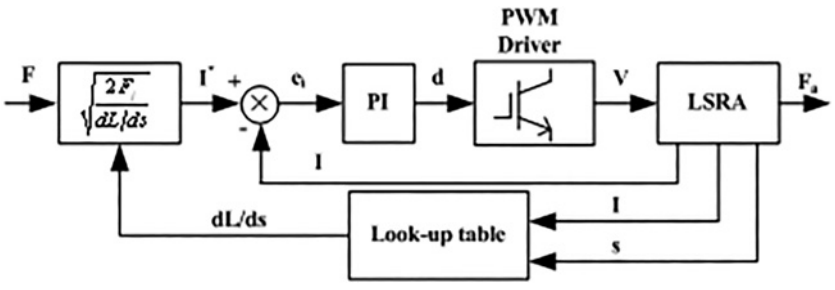

Fig. 6 *LSRA direct drive diagram*

doi: 10.1049/iet-epa.2014.0115

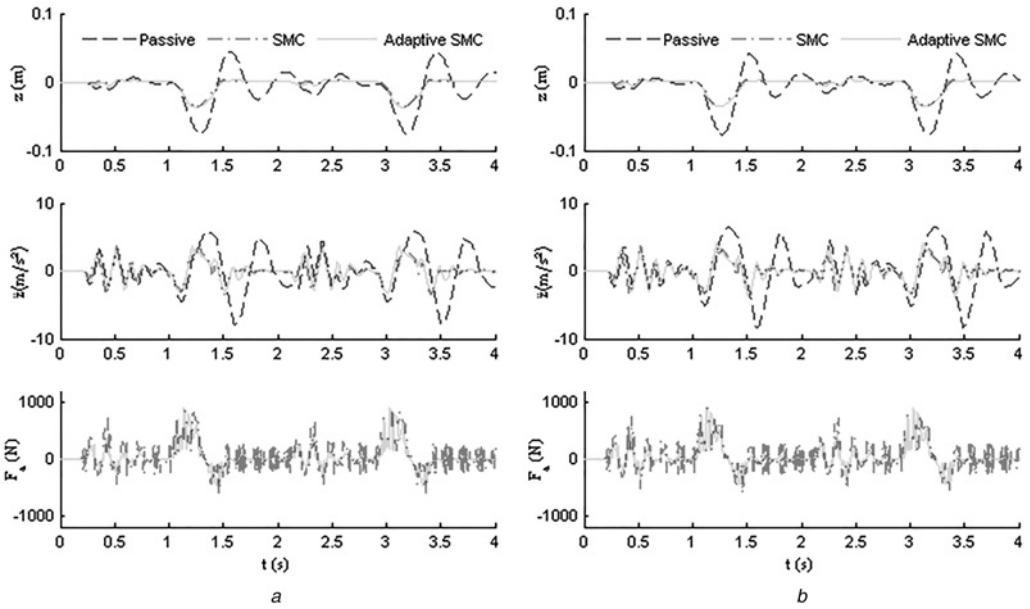

Fig. 7 *Simulated performance of adaptive SMC-based active suspension system with different M_s*

a $M_s = 100\%M_{s0}$
b $M_s = 80\%M_{s0}$

In this research, the car passes through three bumps that shown in Fig 3b at the speed of 1 m/s, and the output force F_a of LSRA is restricted within [−900 N, 900 N]. The performance of the proposed adaptive SMC scheme is illustrated in Fig. 7 with regard to load variation, comparing with the SMC without adaptation mechanism. It can be seen from simulation results that the behaviours under SMC and adaptive SMC are similar, and the performances of both cases are improved significantly with respect to passive suspension. In this paper, nominal and light loads are considered in the laboratory test. For the nominal load system, the displacement of the car body of adaptive SMC increases up to 0.03 m at the time instant of 1.25 s and return to zero at the time instant of 1.45 s shown in Fig. 7*a*, while the car body with only passive suspension oscillates for 1.5 s and its amplitude is up to 0.08 m. The difference shows the effectiveness of the proposed controller. The amplitude of acceleration of the car body of active suspension system is half of that of passive suspension, indicates that the riding comfort has been improved. The active force generated by the LSRA is within the mechanical limitation as shown in the bottom of Fig. 7*a*.

The responses of the passive and active suspension system with regard to light load are similar to the nominal case. As shown in Fig. 7*b*, the displacement and acceleration of the car body of active suspension are constrained by 0.035 m and 4 m/s^2, respectively. The peak values are decreased significantly in comparison with the passive suspension.

From the simulation results, both the SMC and adaptive SMC can improve the dynamic performances of the active suspension system. The main difference between two methods with and without adaptation mechanism is that the generated active force F_a. It can be observed that the active force under adaptation mechanism reaches its peak value when the largest displacement and acceleration are large and keeps at a small range in the rest of the period. In contrast, the active force without adaptation mechanism generates large force when the displacement and acceleration are relatively small that implied the SMC is too sensitive to road variation. It can be concluded that both control methods achieve good performance with regard to load variation and road profile, and the SMC with adaptation mechanism consumes less power and is more effective.

To verify the effectiveness of the proposed adaptive sliding mode controller, experiments of the active suspension system with regard to nominal and light load are carried out in the laboratory test platform. The experiment results shown in Fig. 8 examine the superior performance of the proposed active suspension system. In both cases, the car body starts to oscillate when the car encounters the big bump at the time instant of 1 s. The amplitudes of displacement and acceleration are up to 0.08 m and 8 m/s^2, respectively. Moreover, the decay processes are slow and the car vibration lasts for over 1.5 s. The performance of the active suspension system has been improved significantly with LSRA. When the wheel passes over a bump, the car body falls and the LSRA generates compensation force based on the proposed control scheme. The amplitudes of displacement and acceleration of the car body under nominal load are about 0.032 m and 4 m/s^2, respectively. The slight difference between experimental results and simulation results are reasonable because of real-time implementation constraints and LSRA characteristics. Nevertheless, the peak values of displacement and acceleration in both nominal load case and light load case are decreased significantly up to half of those of the passive suspension. The improved performance of the proposed active suspension system is verified.

7 Conclusion

An adaptive sliding mode controller has been developed in this paper for a quarter-car active suspension system with LSRA. A non-linear model is used to describe the suspension system with the consideration of spring non-linearity. The system non-linearities and external road disturbance can be estimated by the adaptive mechanism for the purpose of global stability, including the force

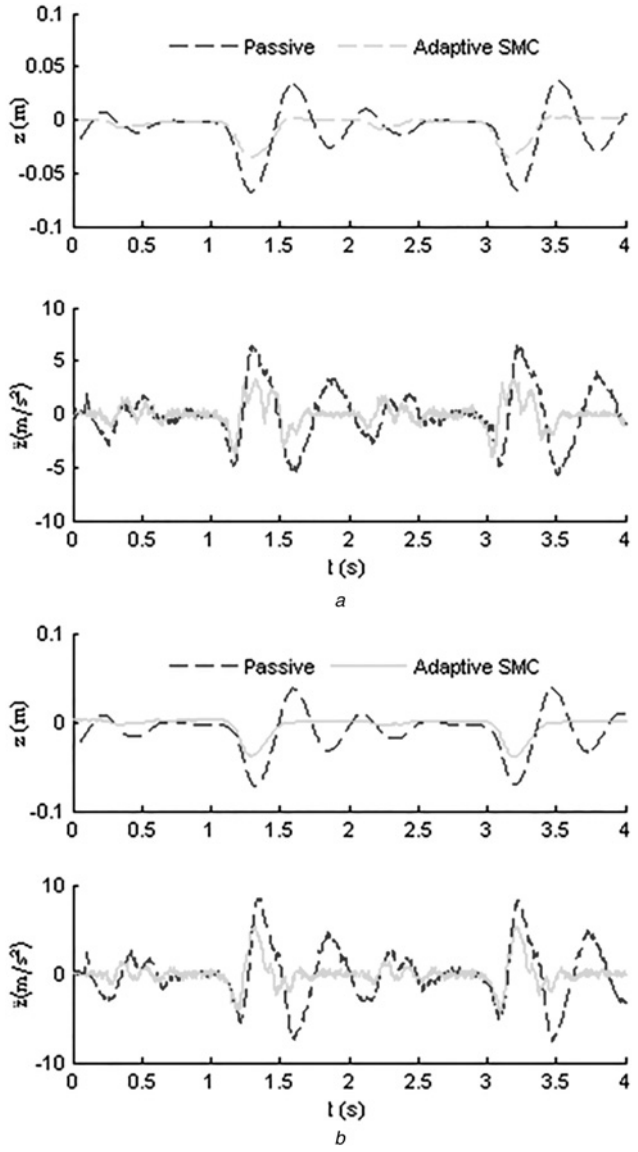

Fig. 8 *Experimental results of adaptive SMC-based active suspension system with reference to load variation*

a $M_s = 100\%M_{s0}$
b $M_s = 80\%M_{s0}$

uncertainties because of LSRA non-linearities. Sliding mode control technique is employed to ensure the global stability of the quarter-car active suspension system and stabilise the car body with only position and velocity feedback of the car body. Both sliding mode control methods, with and without adaptation mechanism, perform similar dynamic behaviours of vehicle vertical motion and provide better responses with regard to passive suspension system demonstrated in simulation results. The main difference between two SMCs is that adaptive SMC achieves better force output efficiency than that of conventional SMC. By applying the proposed adaptive SMC, the ride comfort can be improved significantly that has been examined by experimental results.

8 Acknowledgment

The authors gratefully acknowledge the financial support of the Innovation and Technology Fund (ITP02509AP).

9 References

1 Brezas, P., Smith, M.C.: 'Linear quadratic optimal and risk-sensitive control for vehicle active suspensions', *IEEE Trans. Control Syst. Technol.*, 2014, **22**, (2), pp. 543–556
2 Li, H., Yu, J., Hilton, C., Liu, H.: 'Adaptive sliding-mode control for nonlinear active suspension vehicle systems using T–S fuzzy approach', *IEEE Trans. Ind. Electron.*, 2013, **60**, (8), pp. 3328–3338
3 Lin, J.K., Cheng, K.W.E., Zhang, Z., Cheung, N., Xue, X.D., Ng, T.W.: 'Active suspension system based on linear switched reluctance actuator and control schemes', *IEEE Trans. Veh. Technol.*, 2013, **62**, (2), pp. 562–572
4 Bryant, A., Beno, J., Weeks, D.: 'Benefits of electronically controlled active electromechanical suspension systems (EMS) for mast mounted sensor packages on large off-road', SAE Technical Paper, 2011, no. 2011-01-0269
5 Gysen, B.L.J., Paulides, J.J.H., Janssen, J.L.G., Lomonova, E.A.: 'Active electromagnetic suspension system for improved vehicle dynamics', *IEEE Trans. Veh. Technol.*, 2010, **59**, (3), pp. 1156–1163
6 Karnopp, D.: 'Permanent magnet linear motors used as variable mechanical dampers for vehicle suspensions', *Veh. Syst. Dyn.*, 1989, **18**, (4), pp. 187–200
7 Wang, J., Wang, W., Atallah, K.: 'A linear permanent-magnet motor for active vehicle suspension', *IEEE Trans. Veh. Technol.*, 2011, **60**, (1), pp. 55–63
8 Lee, S., Kim, W.-j.: 'Active suspension control with direct-drive tubular linear brushless permanent-magnet motor', *IEEE Trans. Control Syst. Technol.*, 2010, **18**, (4), pp. 859–870
9 Zhang, Z., Cheung, N.C., Cheng, K.W.E., Xue, X., Lin, J.: 'Direct instantaneous force control with improved efficiency for four-quadrant operation of linear switched reluctance actuator in active suspension system', *IEEE Trans. Veh. Technol.*, 2012, **61**, (4), pp. 1567–1576
10 Martins, I., Esteves, J., Pina da Silva, F., Verdelho, P.: 'Electromagnetic hybrid active-passive vehicle suspension system'. IEEE 49th Vehicular Technology Conf., 1999, pp. 2273–2277
11 Gysen, B.L.J., van der Sande, T.P.J., Paulides, J.J.H., Lomonova, E.A.: 'Efficiency of a regenerative direct-drive electromagnetic active suspension', *IEEE Trans. Veh. Technol.*, 2011, **60**, (4), pp. 1384–1393
12 Weeks, D., Bresie, D., Beno, J., Guenin, A.: "The design of an Electromagnetic Linear Actuator for an Active Suspension", *SAE Technical Paper 1999-01-0730*, Mar 1999, SAE International Congress & Exposition, Detroit, USA
13 Kim, Y., Hwang, W., Kee, C., Yi, H.: 'Active vibration control of a suspension system using an electromagnetic damper', *Proc. Inst. Mech. Eng. Pt. D: J. Automob. Eng.*, 2001, **215**, (8), pp. 865–873
14 Boldea, I., Nasar, S.A.: 'Linear motion electromagnetic devices' (Taylor & Francis, 2001, 1st edn.)
15 Pan, J.F., Zou, Y., Cheung, N.C.: 'Performance analysis and decoupling control of an integrated Rotary–Linear machine with coupled magnetic paths', *IEEE Trans. Magn.*, 2014, **50**, (2), pp. 761–764
16 Rallabandi, V., Fernandes, B.G.: 'Design procedure of segmented rotor switched reluctance motor for direct drive applications', *IET Electr. Power Appl.*, 2014, **8**, (3), pp. 77–88
17 Garcia-Amorós, J., Blanqué Molina, B., Andrada, P.: 'Modelling and simulation of a linear switched reluctance force actuator', *IET Electr. Power Appl.*, 2013, **7**, (5), pp. 350–359
18 Ding, W., Liu, L., Lou, J.: 'Design and control of a high-speed switched reluctance machine with conical magnetic bearings for aircraft application', *IET Electr. Power Appl.*, 2013, **7**, (3), pp. 179–190
19 Chang, Y.-T., Cheng, K.W.E.: 'Sensorless position estimation of switched reluctance motor at startup using quadratic polynomial regression', *IET Electr. Power Appl.*, 2013, **7**, (7), pp. 618–626
20 Chen, P., Huang, A.: 'Adaptive sliding control of non-autonomous active suspension systems with time-varying loadings', *J. Sound Vibrat.*, 2005, **282**, (3), pp. 1119–1135
21 Utkin, V.I., Guldner, J., Shi, J.: 'Sliding mode control in electro-mechanical systems' (CRC Press, Boca Raton, FL, 2009, 2nd edn.)
22 Slotine, J.E., Li, W.: 'Applied nonlinear control' (Prentice Hall, New Jersey, 1991, 1st edn.)
23 Åström, K.J., Wittenmark, B.: 'Adaptive control' (Dover Publications, 2008, 2nd edn.)
24 Levant, A.: 'Principles of 2-sliding mode design', *Automatica*, 2007, **43**, (4), pp. 576–586
25 Sam, Y.M., Osman, J.H.S., Ghani, M.R.A.: 'A class of proportional integral sliding mode control with application to active suspension system', *Syst. Control Lett.*, 2004, **51**, (3–4), pp. 217–223
26 Xiao, J., Kulakowski, B.T.: 'Sliding mode control of active suspension for transit buses based on a novel air-spring model'. IEEE Proc. of the American Control Conf., 2003, pp. 3768–3773

doi: 10.1049/iet-epa.2014.0115

27 Moradi, M., Fekih, A.: 'Adaptive PID-sliding-mode fault-tolerant control approach for vehicle suspension systems subject to actuator faults', *IEEE Trans. Veh. Technol.*, 2014, **63**, (3), pp. 1041–1054
28 Cao, W., Xu, J.: 'Nonlinear integral-type sliding surface for both matched and unmatched uncertain systems', *IEEE Trans. Autom. Control*, 2004, **49**, (8), pp. 1355–1360
29 Lascu, C., Boldea, I., Blaabjerg, F.: 'Super-twisting sliding mode control of torque and flux in permanent magnet synchronous machine drives'. Industrial Electronics Society, IECON 2013–39th Annual Conf. of the IEEE, 2013, pp. 3171–3176
30 Lian, R.-J.: 'Enhanced adaptive self-organizing fuzzy sliding-mode controller for active suspension systems', *IEEE Trans. Ind. Electron.*, 2013, **60**, (3), pp. 958–968
31 Zhang, Z.: 'Application of linear switched reluctance actuator in active suspension systems', PhD Thesis, Hong Kong, Dept. of Electrical Engineering, Hong Kong Polytechnic University, Hong Kong, 2012
32 Åström, K., Hägglund, T.: 'Revisiting the Ziegler–Nichols step response method for PID control', *J. Process Control*, 2004, **14**, (6), pp. 635–650

10 Appendix

10.1 Appendix 1: system parameters

ASS

$M_{s0} = 110$ kg
$M_u = 90$ kg
$K_{1s} = 18\,600$ N/m
$K_{2s} = 150\,000$ N/m
$C_s = 600$ Nsm^{-1}
$K_u = 160\,000$ N/m
$C_u = 150$ Nsm^{-1}

LSRA

$R_s = 0.5\ \Omega$
$F_{a\max} = 900$N